magnetochemistry

MDPI

Article

Synergistic Enhancement of Tb Diffusion Efficiency in Nd-Ce-Fe-B-Sintered Magnets by Ferromagnetic Elements of Fe and Ni

Qing Feng [1], Xuhang Zhang [1,2,*], Yaxiang Wu [1], Mingpeng Kou [1], Wanqi Qiu [1], Na He [1], Hongya Yu [1] and Zhongwu Liu [1,*]

[1] School of Materials Science and Engineering, South China University of Technology, Guangzhou 510640, China; fq_xhy@163.com (Q.F.); yaxiang@scut.edu.cn (Y.W.); mpkou1023@163.com (M.K.); mewqqiu@scut.edu.cn (W.Q.); clhn@scut.edu.cn (N.H.); yuhongya@scut.edu.cn (H.Y.)

[2] School of Electronic Science and Engineering, Xi'an Jiaotong University, Xi'an 710049, China

* Correspondence: 17788182573@163.com (X.Z.); zwliu@scut.edu.cn (Z.L.)

Abstract

Improving heavy rare-earth (HRE) diffusion efficiency is one of the key issues for the application of grain boundary diffusion in Nd-Ce-Fe-B-sintered magnets. Here, the diffusion efficiency of Tb is significantly enhanced by alloying Tb with ferromagnetic elements Fe and Ni, offering an alternative to conventional strategies based mainly on low-melting-point element additions. Starting from the $Tb_{70}Fe_{30}$ binary alloy, the composition of the diffusion source is systematically optimized by substituting Fe with Ni, which further lowers the melting point of the diffusion alloy. $Tb_{70}Fe_{15}Ni_{15}$ diffusion increased the coercivity of the magnet from 986 kA/m to 1939 kA/m, corresponding to an enhancement of 96.7%. Microstructural observations reveal that the incorporation of Fe and Ni can remarkably promote inward Tb diffusion into the magnet, leading to the formation of deeper Tb-rich shells, which is responsible for the significant coercivity enhancement. Meanwhile, Ni preferentially segregates into the intergranular phases, where two Ni-rich phases with amorphous and cubic structures are formed in the $Tb_{70}Fe_{15}Ni_{15}$-diffused magnet. This work provides new insights into the role of ferromagnetic elements in regulating HRE diffusion and offers a potential strategy for diffusion-source composition design.

Keywords: Nd-Ce-Fe-B sintered magnets; grain boundary diffusion process; ferromagnetic elements; coercivity

Check for updates

Academic Editor: João Carlos Bentes Waerenborgh

Received: 20 October 2026
Revised: 9 November 2026
Accepted: 14 November 2026
Published: 17 November 2026

Copyright: © 2026 by the authors. Licensee MDPI, Basel, Switzerland. This article is an open access article distributed under the terms and conditions of the Creative Commons Attribution (CC BY) license.

1. Introduction

Nd-Fe-B permanent magnets serve as critical components in green energy technologies owing to their unparalleled magnetic performance, especially in wind turbine generators and electric vehicle traction motors [1,2]. Currently, most sintered Nd-Fe-B magnets without heavy rare earth (HRE) addition exhibit insufficient coercivity (typically < 1600 kA/m) to meet practical requirements for high-temperature applications. The coercivity of permanent magnets is closely related to their magnetization-reversal behavior, which can be significantly influenced by local compositional and structural inhomogeneities. Previous studies have demonstrated that structural modulation and compositional variations can alter the magnetization-reversal process and consequently affect the coercivity [3,4]. Therefore, introducing HRE elements into the magnets to enhance coercivity is critically important for

expanding their application field [5]. To reduce the severe decrease in remanence caused by antiferromagnetic coupling between HREs and Fe, grain boundary diffusion (GBD) technology was proposed to minimize HRE incorporation [6–10]. Extensive efforts have been devoted to further improving HRE diffusion efficiency, primarily focusing on matrix modification and diffusion source optimization [5,11–15].

Conventionally, the addition of high-abundance Ce to magnets is considered harmful to magnetic performance because $Ce_2Fe_{14}B$ alloys exhibit inferior intrinsic properties compared to $Nd_2Fe_{14}B$ [16–20]. However, recent studies have revealed that a small amount of Ce substitution in Nd-Fe-B magnets can provide additional low-melting-point diffusion channels for HRE elements, thereby significantly enhancing their diffusion efficiency [21]. Consequently, the slight degradation in coercivity caused by Ce substitution can be effectively counterbalanced by the increased coercivity by diffusion treatment. This not only ensures sufficient magnetic performance but also reduces the material cost. We previously carried out a systematic investigation [22,23] on GBD of sintered Nd-Fe-B magnet by the binary Tb-M alloy diffusion sources. It was found that Tb-Fe diffusion can significantly enhance the coercivity of the magnet with 8 wt.% Ce substitution for Nd. After Tb-Fe diffusion, the magnet exhibited a coercivity of 1711 kA/m, surpassing the value of 1689 kA/m observed in the Ce-free magnet [23]. However, despite this progress, the coercivity enhancement is still inferior to those reported for the Nd-Fe-B magnets treated by many other Tb-based alloy diffusion sources, likely due to the insufficient diffusion efficiency of the Tb-Fe alloy [24–26].

It is generally accepted that low-melting-point elements such as Al [27,28], Cu [14,29,30], and Ga [26] can improve grain boundary wettability, thereby enhancing the diffusion efficiency of HRE elements. Studies have shown that ferromagnetic elements such as Co and Ni not only increase the Curie temperature of the main phase but also promote HRE diffusion, with Ni exhibiting particularly high efficiency [31–34]. Our previous work [34] further confirmed that Ni predominantly diffuses along grain boundaries, creating additional highly active diffusion pathways for HRE elements. Hence, this work incorporates Ni into the diffusion source, and the effects of various Ni doping on the magnetic properties and microstructural evolution of GBD-processed magnets have been systematically investigated. The results reveal that optimal Ni introduction significantly increases HRE diffusion depth and maximizes coercivity enhancement, highlighting the effectiveness of ferromagnetic elements in regulating HRE diffusion.

2. Materials and Methods

A commercial N48 Nd-Ce-Fe-B-sintered magnet (Ce/TRE = 8.45 wt.%, TRE = total rare earth) was used as the initial material for GBD. The initial magnet was cut into cylindrical shapes with dimensions of $\Phi 10 \times 5$ mm^3, after which they were polished and prepared for GBD treatment. The 5 mm thickness is aligned with the c-axis. The diffusion sources with the compositions of $Tb_{70}Fe_{30-x}Ni_x$ (x = 0, 10, 15, 20, and 30, at.%) were prepared by arc-melting and melt-spinning. For simplicity, these diffusion sources were labeled as TbFe, TbFeNi10, TbFeNi15, TbFeNi20, and TbNi. Subsequently, the ribbons were milled into powders with particle size of 150 μm. Diffusion slurries were prepared by mixing the fine powders with alcohol and polyvinyl alcohol (PVA), then coated on the two pole surfaces of the magnets. The usage of Tb in each sample was 1.2 wt.%. The coated magnets underwent a diffusion heat treatment at 900 °C for 6 h, followed by annealing at 500 °C for 3 h.

The melting point Tm of the diffusion source was determined using differential scanning calorimetry (DSC 404F3, NETZSCH-Gerätebau GmbH, Selb, Germany). The magnetic properties were evaluated using a permanent magnetic measurement system (MATS-2010H, Hunan Lianzhong Technology Co., Ltd., Loudi, China). The phase composition of the mag-

nets was characterized by X-ray diffraction (XRD, PANalytical, Almelo, The Netherlands) with Cu Kα radiation. Microstructural evolutions were examined via scanning electron microscopy (SEM, Nova NanoSEM, Thermo Fisher Scientific, Waltham, MA, USA) and transmission electron microscopy (TEM, Talos F200x, Thermo Fisher Scientific, Waltham, MA, USA), and the elemental distributions were detected by an electron probe microanalyser (EPMA, EPMA-1720H, Shimadzu Corporation, Kyoto, Japan).

3. Results and Discussion

Figure 1a shows the DSC curves of $Tb_{70}Fe_{30-x}Ni_x$ alloys at the temperature range of 500–900 °C. The TbFe alloy exhibits a single endothermic peak at 855 °C corresponding to its melting point, while Ni addition significantly reduces the melting point of the diffusion alloy. Specifically, both TbFeNi15 and TbFeNi20 exhibit identical melting point at 750 °C, whereas the TbNi alloy shows two endothermic peaks at 720 °C and 765 °C. Figure 1b displays the demagnetization curves of different magnets, and Figure 1c presents the coercivity values, providing an intuitive visual comparison. Additionally, the detailed magnetic properties are summarized in Table S1. All diffused magnets exhibit a significant enhanced coercivity compared to the initial magnet. Notably, when an appropriate amount of Ni is introduced into the diffusion source, the TbFeNi10 and TbFeNi15 diffused magnets exhibit significantly higher coercivity, reaching 1919 kA/m and 1939 kA/m, respectively. Further increasing the Ni concentration beyond this optimal level leads to a gradual coercivity reduction. Notably, despite having the same melting temperature of 750 °C, TbFeNi15 diffused magnet exhibits higher coercivity than that of TbFeNi20 diffused magnet. Moreover, TbNi has a lower melting temperature but does not achieve the highest coercivity. These results demonstrate that melting temperature alone cannot account for the composition-dependent coercivity enhancement. The coercivity enhancement normalized by the nominal Tb loading is presented in Figure 1d and reaches a maximum of 794.3 $kA{\cdot}m^{-1}$/wt.% for the TbFeNi15-diffused magnet.

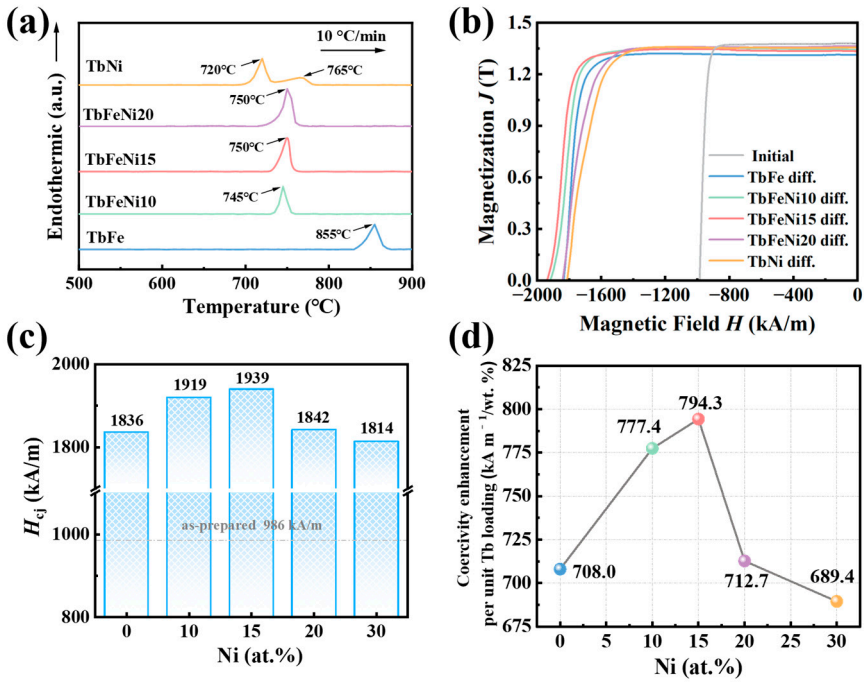


Figure 1. (**a**) DSC curves of $Tb_{70}Fe_{30-x}Ni_x$ alloys at the temperature range of 500–900 °C. (**b**) Demagnetization curves of the initial magnet and $Tb_{70}Fe_{30-x}Ni_x$-diffused magnets. (**c**) Coercivity histogram of the diffused magnets and (**d**) coercivity increment per unit Tb loading.

Detailed microstructural characterization was performed on magnets diffused with three representative compositions (TbFe, TbFeNi15 and TbNi) to elucidate the respective effects of Fe, Ni and combined Fe-Ni additions on Tb diffusion behavior. Figure 2 displays the XRD patterns of the initial magnet and TbFe-, TbFeNi15-, TbNi-diffused magnets. All magnets exhibit strong magnetic anisotropy, and the $Nd_2Fe_{14}B$-type phase (2:14:1 phase) shows strong (0 0 X) orientation. In addition, a satellite peak can be observed right next to the (0 0 6) peak, as shown in Figure 2b. This is primarily attributed to the formation of the $(Nd, Ce, Tb)_2Fe_{14}B$ layer on the grain surface. Tb (0.178 nm) has a smaller atomic radius than that of Nd (0.182 nm), leading to lattice contraction of the 2:14:1 phase [35].

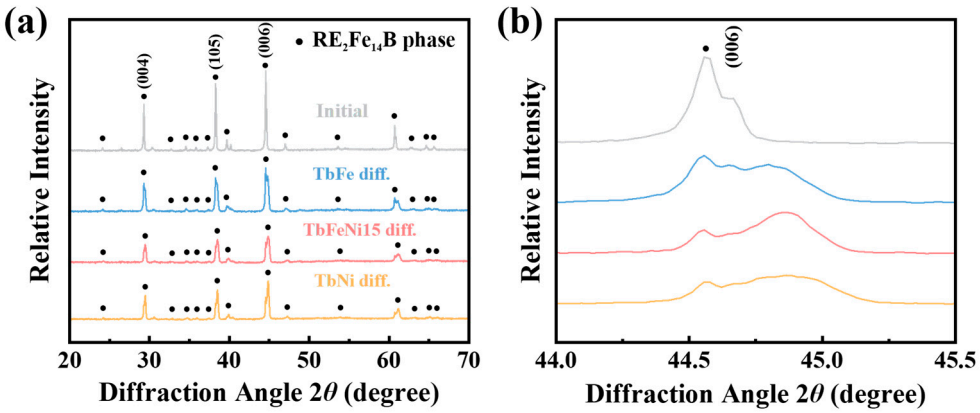


Figure 2. (**a**) XRD patterns of the initial and TbFe-, TbFeNi15-, TbNi-diffused magnets, and (**b**) enlarged patterns in the range of 44.0°to 45.5°.

Figure 3 presents the backscattered scanning microscopy (BSE-SEM) images of TbFe-, TbFeNi15- and TbNi-diffused magnets, illustrating the microstructural evolution at various depths from the diffusion surface. All samples exhibit three distinct regions, indicating different phases. The bright white and dark regions are RE-rich phase and 2:14:1 phase grains. The intermediate gray Tb-rich shells are surrounding the 2:14:1 grains. However, the depth-dependent distribution of Tb-rich shells varies substantially among different magnets, which plays a key role in determining their coercivity. For TbFe-diffused magnets (Figure 3(a–a3)), the Tb-rich shell extends only to approximately 200 μm from the diffusion surface. As the diffusion depth increases to 300 and 500 μm, no obvious shell structure can be observed. For the TbNi-diffused magnets (Figure 3(c–c3)), the Tb-rich shells are notably thick within 200 μm from the diffusion surface, and localized Tb-rich grains are observed, as highlighted by the white dashed box in Figure 3c. The excessive consumption of Tb near the surface severely restricts its inward diffusion into the magnet. As a result, the Tb-rich shell becomes discontinuous at 300 μm depth and eventually becomes undetectable beyond 500 μm. Interestingly, TbFeNi15-diffused magnets exhibit uniformly thick Tb-rich shell observable at the 300 μm depth from the diffusion surface, and distinct shell layer can still be observed even at 500 μm, as indicated by white arrows in Figure 3(b3). These widely distributed shells with high anisotropy field fundamentally account for the maximized coercivity enhancement in TbFeNi15-diffused magnet. Low-magnification EPMA elemental mappings provide a more direct visualization of the spatial distribution of Tb in the magnet and further clarify the differences in Tb diffusion behavior among the three samples. The TbFe-diffused magnet exhibits a highly inhomogeneous distribution of Tb signals, indicating nonuniform formation of Tb-rich shells, as shown in Figure 3d. The TbNi-diffused magnet (Figure 3f) shows substantial Tb accumulation near the diffusion surface. In contrast, the TbFeNi15-diffused magnet exhibits less pronounced Tb enrichment near the diffusion surface than the TbNi-diffused magnet, together with a more homogeneous, network-

like distribution of Tb signals than the TbFe-diffused magnet. Previous micromagnetic simulations [36] have shown that the formation of HRE-rich shells in diffusion-treated magnets shifts the preferred reverse-domain nucleation sites toward the undiffused central region of the magnet. Moreover, the high H_A of the HRE-rich shells impedes the propagation of reversed domains between adjacent grains, thereby enhancing coercivity.

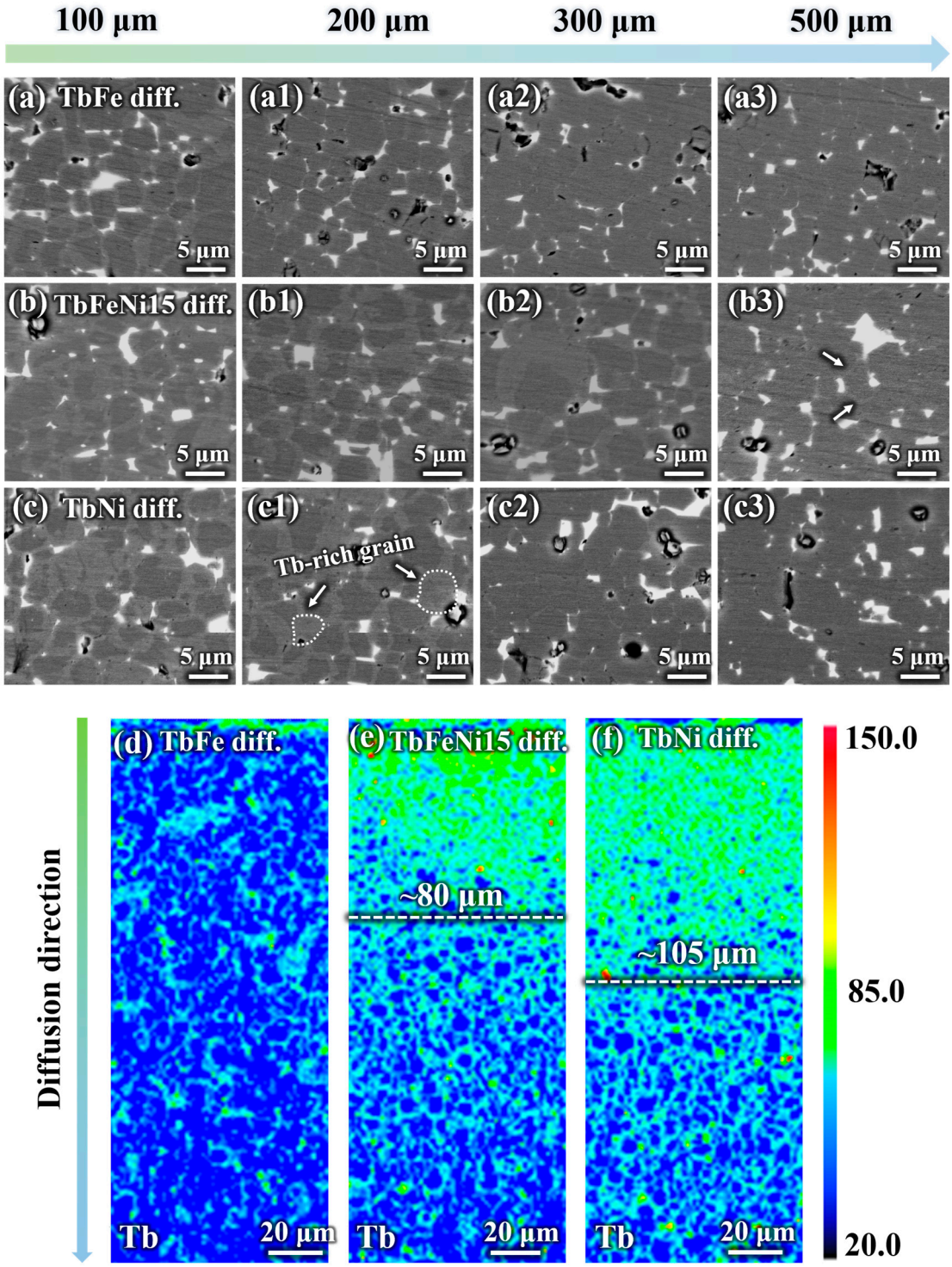


Figure 3. BSE-SEM images of the TbFe- (**a**–**a3**), TbFeNi15- (**b**–**b3**) and TbNi (**c**–**c3**)-diffused magnets at diffusion depths of 100–500 μm. Low-magnification EPMA mappings of Tb element for the TbFe- (**d**), TbFeNi15- (**e**) and TbNi (**f**) -diffused magnets.

Figure 4 provides high-magnification EPMA elemental mappings at the depth of 150 μm from diffusion surface for the TbFe-, TbFeNi15- and TbNi-diffused magnets. At this depth, Tb-rich shells are observed in all magnets, serving as the primary cause of coercivity enhancement. Nevertheless, pronounced difference in the distribution of Tb-rich shells are evident among three magnets. The blurred and discontinuous shell layer at 150 μm depth in TbFe-diffused magnets indicates the intrinsically low diffusion ability of the Tb-Fe alloy. In contrast, the TbNi-diffused magnet exhibits a clearly observable thick shell layer. Such thick shells accelerate Tb depletion within the near-surface region, thereby hindering Tb inward diffusion [37,38]. Notably, the Tb-rich shell in the TbFeNi15-diffused magnet exhibits a uniform distribution and relatively consistent thickness. Quantitative measurements of the Tb-rich shell thickness further confirm this observation, with the TbFeNi15-diffused magnet exhibiting the smallest standard deviation among the three samples (Figure S1). In addition, it can be observed that Ni is predominantly segregated at grain boundaries. Previous studies have reported that such segregation of Ni not only improves the wettability of grain boundary phases but also enhances their chemical stability [34].

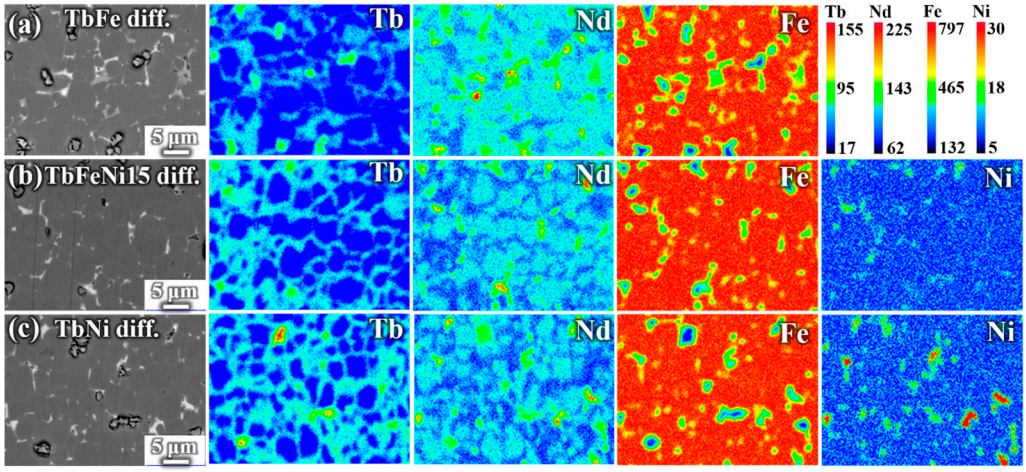


Figure 4. BSE-SEM images and corresponding EPMA elemental mappings of Tb, Nd, Fe and Ni elements at a depth of 150 μm from the diffusion surface for the TbFe- (**a**), TbFeNi15- (**b**) and TbNi (**c**)-diffused magnets.

Figure 5 presents the TEM analysis results of the initial magnet. Figure 5a shows a typical bright-field image of a triple junction grain boundary phase surrounded by three main phase grains, and the $RE_2Fe_{14}B$ main phase structure is confirmed by the selected-area electron diffraction (SAED) pattern shown in Figure 5d. Combined with the fast Fourier transform (FFT) result corresponding to the white dashed box in Figure 5b and the EDS mapping analysis, the triple junction phase can be identified as RE-rich phase with cubic structure. Notably, no precipitation of $CeFe_2$ phase was observed at the grain boundaries due to the relatively low Ce content in this (Nd, Ce)-Fe-B magnet [39,40]. Previous study [21] has demonstrated that such Ce-containing RE-rich phase exhibits a lower melting point than Ce-free RE-rich phase, which can further accelerate the diffusion of HRE elements.

Figure 6 presents the TEM characterization results obtained at 150 μm from the diffusion surface of the TbFeNi15-diffused magnet. Two types of triple junction phases are identified in this region, designated as TJ1 (Figure 6a) and TJ2 (Figure 6d), respectively. Figure 6a shows the bright-field image of the TJ1 phase. Combined with the high-resolution TEM image in Figure 6b and the FFT pattern in Figure 6c, TJ1 can be confirmed to be the same cubic RE-rich phase as that observed in the initial magnet. Based on the high-resolution TEM image (Figure 6e) and FFT image (Figure 6f), the TJ2 region is confirmed to be an amorphous phase. Such an amorphous phase has also been reported previously [34],

and it can reduce the interfacial energy between the main phase and grain boundaries, thereby retarding the nucleation of reversed magnetic domain. Consistently, as revealed by the EDS mapping on the right side, a uniform Tb-rich layer is formed at the periphery of the main phase around both TJ1 and TJ2. The enrichment of Tb is accompanied by a decrease in Nd concentration, which is the main reason for the enhanced coercivity of the TbFeNi15-diffused magnet, since the magnetocrystalline anisotropy field of $Tb_2Fe_{14}B$ is much higher than that of $Nd_2Fe_{14}B$ [16,36].

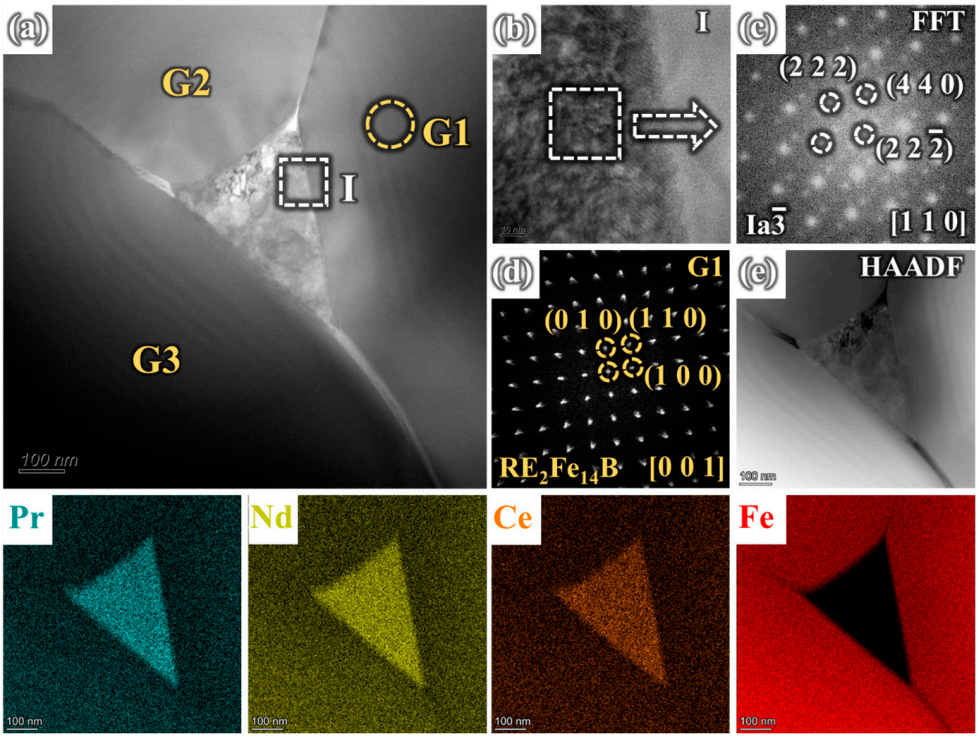


Figure 5. (**a**) Bright-field TEM image of initial magnet. (**b**) HRTEM image of region I in (**a**) and FFT pattern (**c**) corresponding to the white dashed box in (**b**). (**d**) SAED pattern of main phase G1. (**e**) High angle annular dark field (HAADF) image of (**a**) and the corresponding EDS mapping of Pr, Nd, Ce and Fe are shown below.

Generally, alloying HRE metals with low-melting-point elements such as Al [22,26,41–43], Mg [22], Cu [22,30,35,42–44], Zn [22], Mn [22] and Ga [26] is a common strategy for reducing the melting temperature of diffusion sources and facilitating HRE diffusion. Figure 7 summarizes the coercivity enhancement and final coercivity achieved using various Tb-based diffusion sources. The corresponding experimental details are summarized in Table S2. The substantial coercivity enhancement achieved by these diffusion sources is generally associated with the formation of Tb-rich shells with high H_A, which hinder the nucleation and propagation of reversed domains. In the present work, alloying Tb with the ferromagnetic elements Fe and Ni also achieves a significant coercivity enhancement, reaching a final coercivity of 1939 kA/m. These results highlight the potential of ferromagnetic elements as alloying components in Tb-based diffusion sources and provide an alternative strategy for optimizing HRE diffusion and coercivity enhancement in Nd-Fe-B magnets.

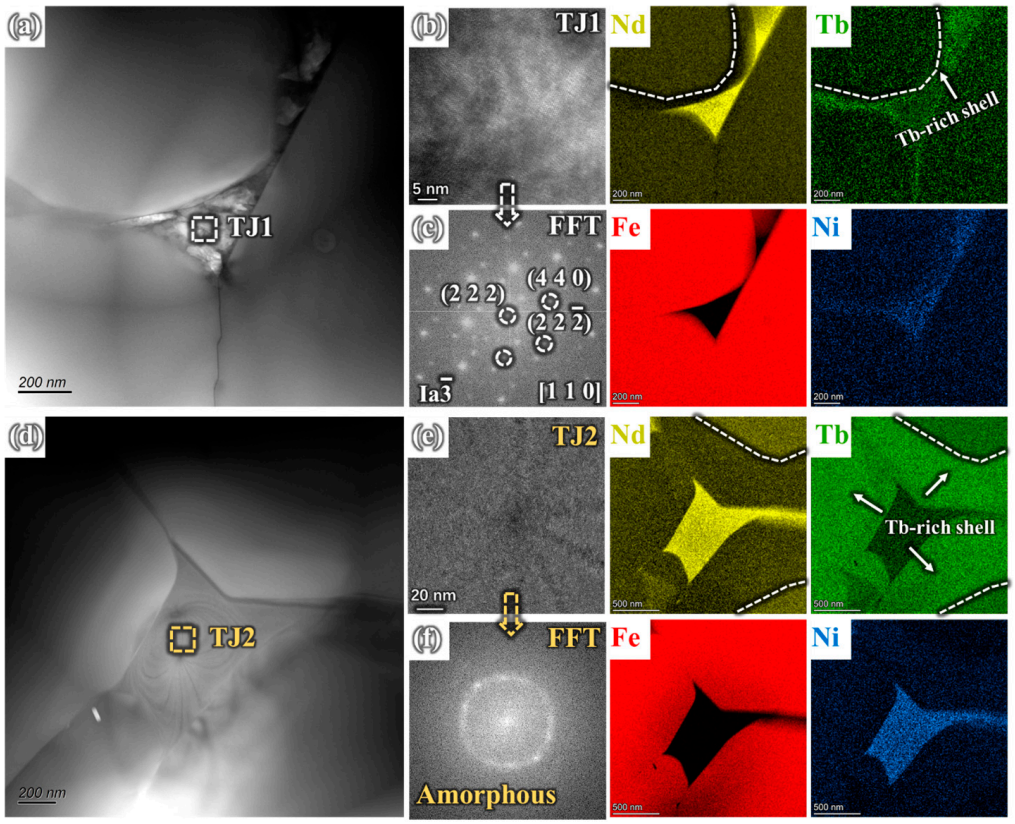


Figure 6. (**a**,**d**) Bright-field TEM images for TbFeNi15-diffused magnet at the depth of 150 μm. (**b**) HRTEM image of TJ1 in (**a**) and corresponding FFT pattern (**c**). (**e**) HRTEM image of TJ2 in (**d**) and corresponding FFT pattern (**f**). The corresponding EDS mappings of Nd, Tb, Fe and Ni are shown on the right side.

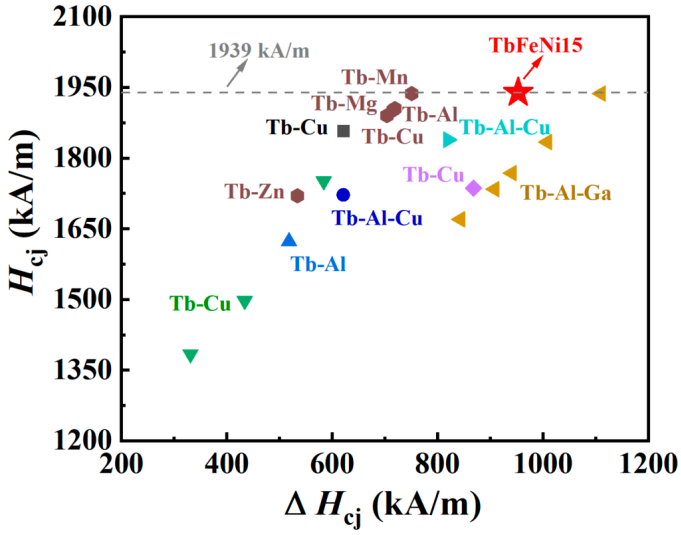


Figure 7. Coercivity enhancement and the final coercivity after diffusion with different Tb-based alloys.

4. Conclusions

In this work, we systematically investigated the effect of $Tb_{70}Fe_{30-x}Ni_x$ alloy diffusion on the magnetic properties of Nd-Ce-Fe-B magnets. The binary Tb-Fe alloy shows low diffusion efficiency due to its relatively high melting point, whereas Tb-Ni alloy diffusion results in severe Tb enrichment on the magnet surface which restricts the diffusion of Tb into

the magnet interior. Tb-Fe-Ni alloys exhibit enhanced diffusion effect. The $Tb_{70}Fe_{15}Ni_{15}$-diffused magnet achieves a coercivity of 1939 kA/m, corresponding to an increase of 96.7% compared with the initial magnet, with only a slight reduction in remanence. Microstructural observations reveal that the formation of a uniform and deep Tb-rich shell inside the magnet is responsible for the significant enhancement of coercivity. The proposed diffusion source design strategy offers an effective route for fabricating high-performance diffused magnets.

Supplementary Materials: The following supporting information can be downloaded at: https://www.mdpi.com/article/10.3390/magnetochemistry12110130/s1. Table S1 Magnetic properties of the initial and $Tb_{70}Fe_{30-x}Ni_x$ diffused magnets. Table S2 Magnetic properties, compositional parameters, and processing conditions of the magnets reported in the literature cited in Figure 7. Figure S1 Tb-rich shell thickness among the TbFe, TbFeNi15 and TbNi magnets obtained from the EPMA results in Figure 4.

Author Contributions: Conceptualization, Q.F. and X.Z.; validation, Y.W. and N.H.; formal analysis, Q.F., X.Z. and M.K.; investigation, N.H., Y.W. and W.Q.; resources, H.Y. and Z.L.; data curation, W.Q.; writing—original draft preparation, Q.F.; writing—review and editing, Z.L.; visualization, Q.F. and X.Z.; supervision, H.Y.; project administration, Z.L.; funding acquisition, Z.L. All authors have read and agreed to the published version of the manuscript.

Funding: This research was funded by National Natural Science Foundation of China, grant number 52571218 and Guangxi Science and Technology Program, grant number 2024AD47008.

Data Availability Statement: All relevant data are within the manuscript, and data available on request from the authors.

Conflicts of Interest: The authors declare no conflicts of interest.

References

1. Wang, Z.; Sasaki, T.T.; Une, Y.; Ohkubo, T. Microstructure–Coercivity Correlation in 3 T-Class Nd–Fe–B Sintered Magnets with Low Tb Content via a Two-Step Grain Boundary Diffusion Process. *Acta Mater.* **2026**, *314*, 122272. [CrossRef]
2. Feng, Q.; Huang, D.; Zhao, L.; Fan, J.; Jin, L.; Pan, Y.; Hong, Y.; Liu, X.; Pan, A.; Jia, H.; et al. Overcoming Refractory $REFe_2$ Phase Bottleneck in High-Ce Nd–Ce–Fe–B Magnets via Praseodymium-Induced Phase Transformation: Enabling Liquid-Phase Grain Boundary Diffusion of Dysprosium. *Adv. Funct. Mater.* **2026**, *36*, e25964. [CrossRef]
3. Sáez, G.; Cisternas, E.; Díaz, P.; Vogel, E.E.; Burr, J.P.; Saavedra, E.; Escrig, J. Tuning the Coercive Field by Controlling the Magnetization Reversal Process in Permalloy Modulated Nanowires. *J. Magn. Magn. Mater.* **2020**, *512*, 167045. [CrossRef]
4. Arciniegas Jaimes, D.M.; Carballo, J.M.; Broens, M.I.; Bruno, M.; Tejo, F.; Saavedra, E.; Escrig, J.; Bajales, N. Magnetic Properties of CoNi Nanowires and Nanotubes: Insights from Micromagnetic Simulations and Composition-Dependent Equations. *Results Phys.* **2023**, *54*, 107082. [CrossRef]
5. Kim, T.-H.; Sasaki, T.T.; Ohkubo, T.; Takada, Y.; Kato, A.; Kaneko, Y.; Hono, K. Microstructure and Coercivity of Grain Boundary Diffusion Processed Dy-Free and Dy-Containing Nd Fe B Sintered Magnets. *Acta Mater.* **2019**, *172*, 139–149. [CrossRef]
6. Kim, T.-H.; Sasaki, T.T.; Koyama, T.; Fujikawa, Y.; Miwa, M.; Enokido, Y.; Ohkubo, T.; Hono, K. Formation Mechanism of Tb-Rich Shell in Grain Boundary Diffusion Processed Nd–Fe–B Sintered Magnets. *Scr. Mater.* **2020**, *178*, 433–437. [CrossRef]
7. Hirota, K.; Nakamura, H.; Minowa, T.; Honshima, M. Coercivity Enhancement by the Grain Boundary Diffusion Process to Nd-Fe-B Sintered Magnets. *IEEE Trans. Magn.* **2006**, *42*, 2909–2911. [CrossRef]
8. Sepehri-Amin, H.; Ohkubo, T.; Hono, K. The Mechanism of Coercivity Enhancement by the Grain Boundary Diffusion Process of Nd–Fe–B Sintered Magnets. *Acta Mater.* **2013**, *61*, 1982–1990. [CrossRef]
9. Guan, Y.W.; Huang, Y.L.; Rao, Q.; Li, W.; Hou, Y.H.; Luo, J.M.; Pang, Z.S.; Mao, H.Y. Investigation on the Grain Boundary Diffusion of Dy_2O_3 Film Prepared by Electrophoretic Deposition for Sintered Nd-Fe-B Magnets. *J. Alloys Compd.* **2021**, *857*, 157606. [CrossRef]
10. Zhou, T.; Qu, P.; Pan, W.; Liu, R.; Li, M.; Rehman, S.U.; Zhong, Z.; Xie, G. Sintered NdFeB Magnets with Tb-Dy Double-Layer Core/Shell Structure Were Fabricated by Double Alloy Method and Grain Boundary Diffusion. *J. Alloys Compd.* **2021**, *856*, 158191. [CrossRef]
11. Cao, X.; Chen, L.; Guo, S.; Fan, F.; Chen, R.; Yan, A. Effect of Rare Earth Content on TbF_3 Diffusion in Sintered Nd–Fe–B Magnets by Electrophoretic Deposition. *Scr. Mater.* **2017**, *131*, 24–28. [CrossRef]

12. Zhong, S.; Yang, M.; Luo, S.; Chen, T.; Rehman, S.U.; Yang, L.; Li, J.; Zou, Z.; Ma, Q.; Yang, B. Homogeneous Transformation of the Grain Boundary Phase and Tb Grain Boundary Diffusion Optimization in Sintered Nd-Fe-B Magnet. *Intermetallics* **2022**, *144*, 107490. [CrossRef]
13. Zhong, S.; Yang, M.; Wang, H.; Rehman, S.U.; Yu, X.; Luo, S.; Li, L.; Li, C.; Xiong, S.; Yang, B. Grain Boundary Diffusion Efficiency of Sintered Nd-Fe-B Magnets by Al, Sn and Zn Addition. *J. Alloys Compd.* **2023**, *967*, 171676. [CrossRef]
14. Chen, X.; Pan, Y.; Gao, T.; Fan, J.; Deng, X.; Liu, X.; Jia, H.; Zhao, L.; He, J.; Zhang, X. Ce-La-Tb-Cu Grain Boundary Diffusion for Nd-Fe-B Magnets: Toward Obtaining High Coercivity and High Electric Resistivity. *J. Alloys Compd.* **2025**, *1031*, 181056. [CrossRef]
15. Cheng, P.; Cao, S.; Ding, G.; Xie, Y.; Zheng, S.; Zheng, B.; Guo, S.; Chen, R.; Huang, H.; Yu, H.; et al. Magnetic Performances and Diffusion Shell-Structures of Nd-Fe-B Sintered Magnets Treated with Grain Boundary Diffusion by Low Dy-Content Multi-Component Alloys. *J. Alloys Compd.* **2025**, *1011*, 178487. [CrossRef]
16. Herbst, J.F. $R_2Fe_{14}B$ Materials: Intrinsic Properties and Technological Aspects. *Rev. Mod. Phys.* **1991**, *63*, 819–898. [CrossRef]
17. Li, Z.; Li, Y.-Q.; Liu, W.-Q.; Wu, D.; Chen, H.; Xia, W.-X.; Yue, M. Origin of Low Coercivity of High La–Ce-Containing Nd–Fe–B Sintered Magnets. *Rare Met.* **2021**, *40*, 180–184. [CrossRef]
18. Xiao, Y. The Effect of Cerium Doping on the Microstructure and Magnetic Domain of (Nd, Ce)-Fe-B Sintered Magnets. *J. Mater. Res.* **2025**, *40*, 1954–1964. [CrossRef]
19. Chen, H.; Li, Y.; Zhang, H.; Liu, W.; Wu, H.; Qin, Y.; Yue, M.; Wei, Q.; Zhang, B.; Di, J. Strategy for Co-Enhancement of Remanence–Coercivity of RE-Fe-B Sintered Magnets with High Ce-Content: Appropriate La Substitution. *Adv. Sci.* **2023**, *10*, 2301312. [CrossRef] [PubMed]
20. Zhu, M.; Han, R.; Li, W.; Huang, S.; Zheng, D.; Song, L.; Shi, X. An Enhanced Coercivity for (CeNdPr)–Fe–B Sintered Magnet Prepared by Structure Design. *IEEE Trans. Magn.* **2015**, *51*, 2104604. [CrossRef]
21. Qin, Y.; Wang, Z.; Liu, W.; Fan, M.; Song, J.; Wang, G.; Chen, H.; Li, Y.; Zhang, L.; Yue, M. Analysis of Mechanism for Effectively Coercivity Increment in (Nd, Ce)-Fe-B Diffusion Magnets. *J. Alloys Compd.* **2024**, *1003*, 175648. [CrossRef]
22. Kou, M.; Zhang, X.; Feng, Q.; Zeng, C.; Chen, S.; Qiu, W.; Liu, Z. Different Diffusion Behaviors of Binary Tb-M (M: Non-Rare Earth Element) Alloys in Grain Boundary Diffused Nd-Fe-B Magnets. *Mater. Charact.* **2026**, *239*, 116759. [CrossRef]
23. Zhang, X.; Zeng, C.; Liao, X.; Zhou, Q.; Qiu, W.; Liu, Z. Optimizing Ce-Doped Nd-Fe-B Magnets for High-Efficient Grain Boundary Diffusion of Tb-Fe Alloy. *Mater. Res. Bull.* **2025**, *185*, 113302. [CrossRef]
24. Liu, M.; Ji, X.; Zhang, L.; Zhao, B. Efficient Co-Diffusion of Tb and Co in a Sintered Nd-Fe-B Magnet by Low-Melting Point Alloys. *Scr. Mater.* **2023**, *235*, 115600. [CrossRef]
25. Luo, T.; Lin, J.; Sun, C.; Ming, X.; Wang, L.; Cheng, J.; Zhang, J.; Shen, B. Optimizing Terbium Content in Tb-Cu-al Grain Boundary Diffusion to Significantly Enhance Coercivity of Nd-Fe-B Sintered Magnets. *J. Rare Earths* **2025**, *44*, 2146–2157. [CrossRef]
26. Song, R.; Feng, H.; Zhao, H.; Liu, F. Microstructure and Magnetic Properties of Grain Boundary Diffused Nd-Fe-B Magnets with Tb-Al-Ga Alloy. *J. Magn. Magn. Mater.* **2023**, *575*, 170744. [CrossRef]
27. Liang, L.; Pan, X.; Xu, X.; Wang, B.; Cao, B.; Ma, P.; Liu, R.; Wang, H. Achieving High Coercivity and Magnetic Energy in Nd-Fe-B Magnets via Combined Dual-Alloy and Grain Boundary Diffusion Using $Tb_{86}Al_7Co_7$. *J. Alloys Compd.* **2025**, *1033*, 180917. [CrossRef]
28. Wang, Z.; Li, Y.; Liu, W.; Wu, H.; Ji, M.; Du, R.; Hao, N.; Yu, M.; Wang, X.; Bian, M.; et al. Performance and Diffusion Optimization Mechanism in Al-Assisted Grain Boundary Diffused Nd–Fe–B Magnets. *J. Mater. Chem. A* **2026**, *14*, 1806–1820. [CrossRef]
29. Wong, Y.J.; Chang, H.W.; Lee, Y.I.; Chang, W.C.; Chiu, C.H.; Mo, C.C. Coercivity Enhancement of Thicker Sintered NdFeB Magnets by Grain Boundary Diffusion with Low-Melting $Tb_{75-x}Ce_xCu_{25}$ (x = 0–45) Alloys. *J. Magn. Magn. Mater.* **2020**, *515*, 167287. [CrossRef]
30. Zhan, H.; Wang, Y.; Peng, C.; Yu, J.; Wang, Z.; Hu, J.; Bai, X.; Luo, Y.; Wang, L. Effect of Multicomponent Tb-Cu Films Diffusion on the Magnetic Properties and Thermal Stability of Sintered Nd-Fe-B Magnets. *J. Alloys Compd.* **2023**, *945*, 169303. [CrossRef]
31. Wu, Y.; Skokov, K.P.; Schäfer, L.; Maccari, F.; Aubert, A.; Rao, Z.; Schweinar, K.; Gault, B.; Xu, H.; Jiang, C.; et al. A Comparative Study of $Nd_{15}Fe_{78}B_7$ and $Nd_{15}Co_{78}B_7$ Systems: Phase Formations and Coercivity Mechanisms. *Acta Mater.* **2022**, *240*, 118311. [CrossRef]
32. Ji, C.; Huang, Y.; An, X.; Geng, Q.; Zheng, Q.; Du, J. High-Performance and High-Temperature-Stable NdFeB Magnets *via* Grain Boundary Diffusion of TbCo-Based Alloys. *J. Alloys Compd.* **2026**, *1065*, 188178. [CrossRef]
33. Kowalczyk, A.; Stefański, P.; Wrzeciono, A.; Szlaferek, A. Structure and Magnetic Properties of $R_2Fe_{14-x}Ni_xB$ Compounds (R = Nd and Gd). *Phys. Status Solidi A* **1989**, *114*, 355–359. [CrossRef]
34. Xu, Y.; Xu, S.; Zhang, X.; Zeng, C.; Chen, S.; Kou, M.; Yu, H.; Wu, Y.; He, J.; Lei, X.; et al. Enhancing the Temperature and Chemical Stability of Sintered Nd-Fe-B Magnets by al and Ni Assisted Tb Grain Boundary Diffusion. *J. Alloys Compd.* **2025**, *1013*, 178656. [CrossRef]
35. Zhao, L.; He, J.; Li, W.; Liu, X.; Zhang, J.; Wen, L.; Zhang, Z.; Hu, J.; Zhang, J.; Liao, X.; et al. Understanding the Role of Element Grain Boundary Diffusion Mechanism in Nd–Fe–B Magnets. *Adv. Funct. Mater.* **2022**, *32*, 2109529. [CrossRef]

36. Qin, C.; Zheng, S.; Liao, X.; Wang, X.; Zeng, W.; Lu, Q.; Chen, D.; Xu, S.; Liu, Z.; Zhou, Q. Comparative Study of Dy and Tb Diffusion Behavior in Grain Boundary Diffusion Processed Nd-Fe-B Sintered Magnets. *J. Mater. Res. Technol.* **2025**, *35*, 3556–3562. [CrossRef]
37. Wang, Z.; Yue, M.; Liu, W.; Li, Y.; Wu, H.; Liu, Y.; Zha, S.; Yi, X.; Zhang, D.; Lu, Q.; et al. Tuning the Distribution of Tb in Nd-Fe-B Sintered Magnet to Overcome the Magnetic Properties Trade-Off. *Scr. Mater.* **2022**, *217*, 114789. [CrossRef]
38. Li, W.; Zhang, Q.; Zhu, Q.; Xiao, S.; Xu, C.; Yang, L.; Zheng, B.; Mao, S.; Song, Z. Formation of Anti-Shell/Core Structure of Heavy Rare Earth Elements (Tb, Dy) in Sintered Nd-Fe-B Magnet after Grain Boundary Diffusion Process. *Scr. Mater.* **2019**, *163*, 40–43. [CrossRef]
39. Jin, J.; Zhang, Z.; Zhao, L.; Peng, B.; Liu, Y.; Greneche, J.-M.; Yan, M. Evolution of $REFe_2$ (RE = Rare Earth) Phase in Nd-Ce-Fe-B Magnets and Resultant Ce Segregation. *Scr. Mater.* **2019**, *170*, 150–155. [CrossRef]
40. Zhang, Y.; Ma, T.; Jin, J.; Li, J.; Wu, C.; Shen, B.; Yan, M. Effects of $REFe_2$ on Microstructure and Magnetic Properties of Nd-Ce-Fe-B Sintered Magnets. *Acta Mater.* **2017**, *128*, 22–30. [CrossRef]
41. Zhou, T.; Guo, Y.; Xie, G.; Rehman, S.U.; Liu, R.; Liu, J.; Qu, P.; Li, M. Coercivity and Thermal Stability Enhancement of NdFeB Magnet by Grain Boundary Diffusion Tb80Al20 Alloys. *Intermetallics* **2021**, *138*, 107335. [CrossRef]
42. He, J.; Hu, J.; Zhou, B.; Jia, H.; Liu, X.; Zhang, Z.; Wen, L.; Zhao, L.; Yu, H.; Zhong, X.; et al. Simultaneous Enhancement of Coercivity and Electric Resistivity of Nd-Fe-B Magnets by Pr-Tb-Al-Cu Synergistic Grain Boundary Diffusion toward High-Temperature Motor Rotors. *J. Mater. Sci. Technol.* **2023**, *154*, 54–64. [CrossRef]
43. Lee, D.H.; Kim, S.C.; Kim, J.; Baek, J.-Y.; Yun, T.-Y.; Kim, J.T.; Kim, S.; Kim, D.; Lee, S.H.; Do, D.; et al. Coercivity and Thermal Stability Enhancement of Nd-Fe-B Sintered Magnets by Grain Boundary Diffusion with Tb-Al-Cu Alloys. *Materialia* **2024**, *36*, 102161. [CrossRef]
44. Zeng, C.; Chen, S.; Feng, Q.; Kou, M.; Yu, H.; Zhong, X.; Liu, Z. Significant Effects of Residual Carbon on the Grain Boundary Diffusion of Nd-Fe-B Magnets. *J. Alloys Compd.* **2026**, *1065*, 188137. [CrossRef]

Disclaimer/Publisher's Note: The statements, opinions and data contained in all publications are solely those of the individual author(s) and contributor(s) and not of MDPI and/or the editor(s). MDPI and/or the editor(s) disclaim responsibility for any injury to people or property resulting from any ideas, methods, instructions or products referred to in the content.